processes

MDPI

Article

Optimization Configuration of Microgrid Under Multiple Operation Strategies Based on HOMER

Hao Ma [1], Kun Zhuang [1], Jie Yang [1], Wenqian Yin [1], Lili Liu [1], Yuping Wu [2] and Jilei Ye [1,*]

[1] School of Energy Science and Engineering, Nanjing Tech University, Nanjing 211816, China; mahao@njtech.edu.cn (H.M.); zk15151838251@163.com (K.Z.); yangjie2195@163.com (J.Y.); wqyin@njtech.edu.cn (W.Y.); liulili@njtech.edu.cn (L.L.)

[2] Confuius Energy Stroage Lab, School of Energy and Environment & Z Energy Stroage Center, Southeast University, Nanjing 210096, China; wuyp@seu.edu.cn

* Correspondence: yejilei@njtech.edu.cn

Abstract

Addressing the challenge of power supply stability caused by the intermittent nature of photovoltaic power generation in off-grid microgrids, this study uses a commercial park in Wuhan as a case study and optimizes the capacity configuration of a photovoltaic–storage–hydrogen fuel cell hybrid microgrid system based on HOMER Pro software. First, a topology of the off-grid microgrid is constructed, comprising photovoltaic (PV), lithium-ion batteries, hydrogen fuel cells, and a diesel generator as backup. The power output characteristics, efficiency curves, and life-cycle cost models of each component are accurately established. On this basis, two typical operation strategies, namely Load Following (LF) and Cycle Charging (CC), are proposed and compared. The influence of different strategies on the optimal capacity configuration and operational economics is systematically analyzed, and the Cycle Charging strategy is identified as the optimal operation strategy for this scenario. Subsequently, a multi-scenario capacity optimization design is further conducted based on the optimal operation strategy. The minimization of net present cost (NPC) is taken as the primary objective, while multiple evaluation indicators such as renewable fraction (RF), levelized cost of electricity (LCOE), energy storage cycle life degradation, and system redundancy rate are comprehensively considered. The results show that, while ensuring 100% power supply reliability, the proposed model reduces the net present cost (NPC) by approximately 14.4% compared with the conventional PV-storage scheme. The renewable fraction (RF) reaches 95.8%, while the reliance on lithium-ion battery capacity is significantly reduced (battery capacity configuration decreased by 24.3%). This effectively extends the energy storage lifespan and enhances the overall economic and environmental benefits. The results provide a theoretical basis and technical reference for the planning and design of off-grid microgrids with high penetration of renewable energy.

Keywords: off-grid microgrid; photovoltaic–storage–hydrogen fuel cell; HOMER Pro; operation strategy; multi-objective capacity configuration

Check for updates

Academic Editor: Massimo Caruso

Received: 22 April 2026
Revised: 2 June 2026
Accepted: 3 June 2026
Published: 4 June 2026

Copyright: © 2026 by the authors. Licensee MDPI, Basel, Switzerland. This article is an open access article distributed under the terms and conditions of the Creative Commons Attribution (CC BY) license.

1. Introduction

Since the beginning of the 21st century, the issues of energy shortage and environmental degradation have become increasingly prominent. The development and utilization of new renewable energy sources have become an important strategy for global sustainable development [1]. As a small-scale power generation and distribution system independent of the main grid, the off-grid microgrid has become a core solution for addressing power

supply challenges in remote areas and ensuring the stable operation of critical loads. Its key feature lies in integrating distributed energy resources such as photovoltaics and wind power with energy storage devices to achieve local energy self-consumption. This approach reduces transmission losses and construction costs in regions where grid extension is costly, such as islands and mountainous areas, while also decreasing dependence on fossil fuels [2]. However, the power supply reliability and stability of off-grid microgrids face multiple technical challenges. The intermittency and fluctuation of distributed energy resources represent the primary difficulty. Among them, solar power output is constrained by solar irradiance, while wind power output fluctuates with wind speed. Such unstable characteristics, combined with the random variation in loads, can easily lead to power imbalance in the system. Furthermore, without the support of the main grid, the coordinated dispatch of distributed energy resources and energy storage devices becomes a critical technical issue. The robustness of existing operation strategies when dealing with complex operating conditions still requires improvement [3].

The HOMER software package, version 3.18.3, serving as a professional optimization tool for renewable energy systems, provides a scientific approach for the optimal design of microgrid systems. Researchers have conducted studies on the optimal design of off-grid microgrid systems using HOMER, and it has been widely applied to remote-area power supply and distributed energy systems [4]. In terms of optimal capacity configuration for off-grid microgrids, Li Chunpeng et al. designed a hybrid power generation system dominated by solar and wind energy, supplemented by a diesel generator [5]. Through simulation and optimization using HOMER, the system was able to meet load demand and achieve an uninterrupted power supply, with the renewable fraction reaching 67% and the excess electricity percentage being only 9.54%. However, studies indicate that under the same resource supply conditions, photovoltaic cells have relatively high costs, and as the input power increases, the cost per kilowatt-hour (kWh) of electricity generated also rises [6]. Liu [7] conducted a multi-objective optimization combined with the entropy weight method. By constructing a decision matrix, normalizing data, and calculating information entropy to determine the weights of indicators, the optimal system configuration was then selected from feasible combinations using HOMER. Taking the standalone photovoltaic/wind/battery/diesel power generation system on Yongxing Island, China, as a case study, it was verified that this approach enhances the objectivity of decision-making [8]. Addressing the optimal dispatch problem of power systems with a high proportion of renewable energy, Zhang et al. [9] utilized the adjustable capacity of loads to explore the value of load adjustability from the perspectives of demand response and reserve. By aggregating load clusters, they reduced operating costs while improving grid reliability and economic efficiency. Dong et al. [10] proposed a joint optimal dispatch method for distributed photovoltaic–storage systems. By constructing an optimal dispatch model and formulating real-time dispatch strategies, they effectively suppressed grid load fluctuations and regulated peak-valley differences, and verified the approach through simulation case studies. Yu et al. [11] proposed an energy scheduling optimization strategy for smart communities based on time-of-use electricity prices, which reduced electricity costs while achieving load peak shaving and valley filling. In addition, Zhang et al. [12] conducted a study on optimal microgrid configuration under multiple scenarios, taking a commercial park in Wuhan as the research object. They pointed out that off-grid microgrids exhibit photovoltaic curtailment. Through the analysis of different scenarios, they determined the optimal configuration that balances economic performance and environmental cleanliness, thereby reducing the system's reliance on energy storage batteries. In terms of regional system optimization and feasibility analysis, Laetitia et al. [13] conducted a study on the energy system of Popova Island in Russia. They employed a Monte Carlo

model to generate prediction intervals for the levelized cost of electricity (LCOE) and define input scenarios for HOMER, ultimately designing a cost-effective system with a low penetration of renewable energy. The analysis indicated that the discount rate is a key factor influencing the optimal system design. Bahramara et al. [14] found that HOMER holds high application value in remote areas of developing countries. It can adapt to loads ranging from 0.626 kW to 2.213×10^6 kW, with photovoltaics being the mainstream renewable energy choice. The standalone operation mode of hybrid renewable energy systems is more prevalent. Halabi et al. [15] conducted a study on a power station in Sabah, using HOMER to optimize the capacity of a photovoltaic/diesel/battery system. They achieved zero emissions with a 100% renewable energy system. The study found that energy storage systems are crucial for reducing energy losses, and that constructing a 100% photovoltaic/battery energy storage combined system is feasible under specific conditions. Karakoulidis et al. [16] designed a standalone system incorporating renewable energy, conventional energy, and multiple energy storage options based on HOMER. The results indicated that although hydrogen systems are technically feasible, they are excessively costly. In contrast, a photovoltaic–diesel–battery system achieves 33.8% fuel savings and is more suitable for standalone applications. Shaahid et al. [17] utilized solar radiation data from the Rafha region to design and optimize a photovoltaic–diesel–battery energy storage system capable of meeting the load demand of Rawdhat Bin Habbas village using HOMER. The system configuration consisted of 2.5 MW of photovoltaics, 4.5 MW of diesel generators, and battery energy storage with 60 min of autonomous operation. Compared with a pure diesel system, the carbon emissions of the proposed system were reduced by approximately 24%.

In addition to HOMER-based case studies, many researchers have investigated the optimization of multiple energy sources in microgrids from the perspectives of system planning, component sizing, techno-economic evaluation, and energy management. Hafez and Bhattacharya developed an optimal planning and design method for renewable-energy-based microgrid supply systems, in which wind turbines, photovoltaic arrays, battery banks, hydro turbines, diesel generators, dump loads, boilers, and AC/DC converters were considered as candidate energy supply options [18]. Chauhan and Saini reviewed integrated renewable energy systems for stand-alone applications and summarized different system configurations, storage options, sizing methodologies, and control strategies [19]. Jung and Villaran studied the optimal planning and design of hybrid renewable energy systems for microgrid applications, emphasizing that the coordinated sizing and operation of distributed energy resources are essential for improving system economy and reliability [20]. More recently, Ishraque et al. evaluated the design and optimization of an islanded hybrid microgrid under different load dispatch strategies by analyzing component sizing, system response, and cost performance [21]. These studies indicate that the optimization of energy sources in microgrids is not limited to the selection of individual components, but increasingly focuses on the coordinated relationship among renewable energy generation, conventional backup units, energy storage systems, dispatch strategies, and multi-objective evaluation.

The operation strategies for off-grid microgrids are optimized based on HOMER, mainly including two typical types: the Load Following (LF) strategy and the Cycle Charging (CC) strategy. In the LF strategy, controllable power sources, such as diesel generators or fuel cells, generate only the power required to meet the remaining load after renewable energy and battery output are considered. In the CC strategy, once the controllable power source is started, it operates at rated or relatively high output, and the surplus electricity after meeting the load demand is used to charge the battery. Therefore, the main difference between the two strategies is whether the controllable power source

only follows the net load or also charges the storage system. The LF strategy is usually suitable for systems with abundant renewable energy resources, because excess renewable power can be stored in batteries and later released during low-generation periods, thereby reducing fuel consumption and operating costs [22]. In contrast, the CC strategy is more suitable for systems with insufficient renewable energy supply, where controllable power sources need to be started more frequently and their surplus generation can be used to support battery charging [23]. Overall, although considerable progress has been made in the optimal sizing and techno-economic evaluation of hybrid energy sources for microgrids, existing studies mainly focus on component capacity optimization, economic feasibility, or single-objective performance comparison. Relatively limited attention has been paid to the adaptability of different practical operation strategies under the same off-grid microgrid topology. In addition, most studies still take economic performance as the core optimization objective, while the coordinated consideration of cleanliness, photovoltaic curtailment, energy storage operating state, and sensitivity of key parameters remains insufficient.

Compared with previous HOMER-based studies, this work focuses on operation-strategy adaptability rather than only obtaining a least-cost configuration. Therefore, the main contribution of this study is not to develop a new optimization algorithm, but to establish a scenario-oriented capacity configuration and evaluation framework for an off-grid photovoltaic–storage–fuel cell microgrid under different practical operation strategies. Specifically, HOMER Pro is used as the simulation and optimization platform, while the research focus is placed on comparing the effects of Load Following (LF) and Cycle Charging (CC) strategies on system capacity configuration, economic performance, renewable energy utilization, carbon emissions, battery operating state, and photovoltaic curtailment. Furthermore, three optimization scenarios are constructed, including economic-priority optimization, renewable energy-priority optimization, and comprehensive economy-cleanliness optimization. By introducing multi-index evaluation and sensitivity analysis of diesel price, load demand, photovoltaic cost, and battery cost, this study aims to provide an engineering-oriented decision basis for the planning and operation strategy selection of off-grid microgrids with high renewable energy penetration.

2. Topology and Characteristics of Off-Grid Microgrid Systems

2.1. Typical Structure of Off-Grid Microgrid Systems

This paper focuses on the optimization of an off-grid photovoltaic–storage-fuel cell microgrid system. The core of the system consists of photovoltaic modules, fuel cells, energy storage battery banks, inverters (including bidirectional DC-DC converters), and AC loads. The system topology is shown in Figure 1. HOMER software is employed to perform capacity configuration optimization, operation strategy formulation, life-cycle economic assessment, and system operational characteristic analysis. The system operation period is set to 20 years, with a preset discount rate of 2% and a device depreciation rate of 8%.

It should be noted that the component equations presented in this section are standard working models commonly used in HOMER-based microgrid simulation, rather than newly derived mathematical models. They are included to clarify the physical basis, parameter settings, and calculation logic of each component, thereby improving the transparency and reproducibility of the modeling process. The novel contribution of this study lies in the scenario-oriented integration and comparative application of these models under different practical operation strategies, rather than in the derivation of individual component equations.

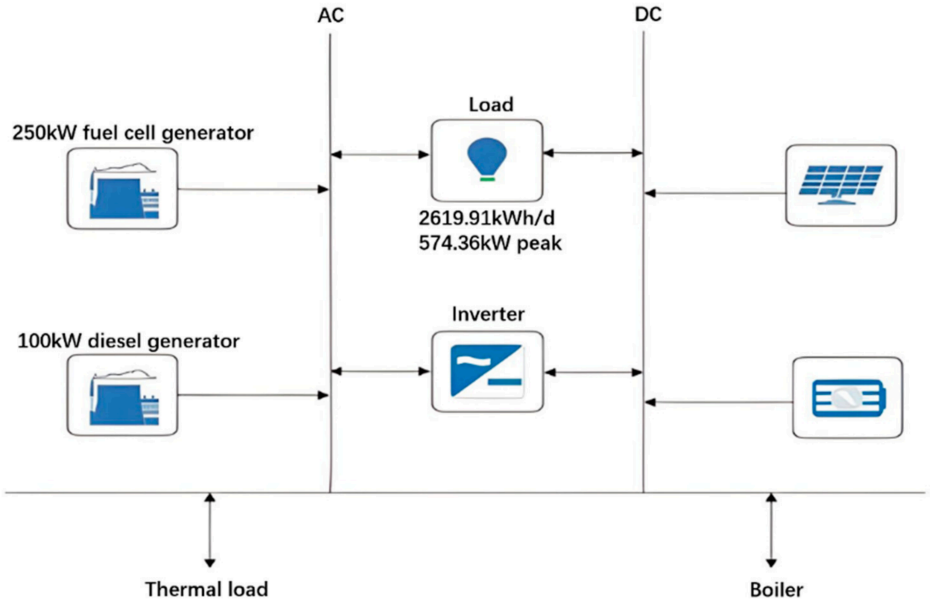


Figure 1. Off-grid PV-battery-fuel cell microgrid system topology.

2.2. Photovoltaic Power Generation Model

The photovoltaic power generation model is expressed in Equation (1), where solar irradiance and photovoltaic array temperature are the core factors affecting the power output. Based on the annual solar irradiance and temperature data at the geographical location of the commercial park, HOMER software systematically analyzes and calculates the annual photovoltaic power generation in this region.

$$P_{PV} = Y_{PV} f_{PV} \left\{ \frac{\overline{G_T}}{\overline{G}_{T,STC}} \right\} [1 + \alpha_P (T_c - T_{c,STC})] \quad (1)$$

where P_{PV} is the output power of the PV panel, Y_{PV} is the PV array output power under standard test conditions (kW), f_{PV} is the PV array derating factor, $\overline{G_T}$ is solar radiation incident on the PV array, $\overline{G}_{T,STC}$ is solar radiation under standard conditions, α_P is the power temperature coefficient, T_c is the PV array temperature, $T_{c,STC}$ is the PV array temperature under standard test conditions.

2.3. Diesel Generator System Model

As an important supplementary power source, the diesel generator plays a key role in meeting peak load demand and addressing the intermittency and instability of photovoltaic power generation caused by meteorological conditions.

The relationship between the fuel consumption of the diesel generator and its power output satisfies the following equation:

$$F_{DG} = aT_{DG} + bP_{DG} \quad (2)$$

where F_{DG} is the fuel consumption rate of the diesel generator (L/h), T_{DG} is the rated capacity of the diesel generator (kVA), P_{DG} is the output power of the diesel generator (kW), a is the intercept of the diesel generator fuel consumption curve (L/kWh), b is the slope of the diesel generator fuel consumption curve (L/kWh).

The efficiency of the diesel generator is expressed as follows:

$$\eta_{DG} = \frac{3600 P_{DG}}{\rho_{DG}(aT_{DG} + bP_{DG})L_{DG}} \quad (3)$$

where η_{DG} is the efficiency of the diesel generator (%), ρ_{DG} is the density of diesel fuel consumed by the diesel generator (kg/m^3), L_{DG} is the lower heating value of diesel fuel consumed by the diesel generator (MJ/kg).

2.4. Energy Storage System Model

In the off-grid photovoltaic–storage–fuel cell microgrid system, the dynamic operating characteristics of the battery are accurately described by the KiBaM model. This model strictly defines the charging and discharging power of the battery under different operating conditions through the following constraint equations:

$$P_{bat,cmax} = \frac{\min(P_{bat,cmax,kbm}, P_{bat,cmax,mcr}, P_{bat,cmax,mcc})}{\eta_{bat,c}} \quad (4)$$

$$P_{bat,dmax} = \eta_{bat,d} P_{bat,dmax,kbm} \quad (5)$$

$$P_{bat,cmax,kbm} = \frac{-kcQ_{max} + kQ_i e^{-k\Delta t} + Qkc(1 - e^{-k\Delta t})}{1 - e^{-k\Delta t} + c(k\Delta t - 1 + e^{-k\Delta t})} \quad (6)$$

$$P_{bac,cmax,mcr} = \frac{(1 - e^{-a_c \Delta t})(Q_{max} - Q)}{\Delta t} \quad (7)$$

$$P_{bat,cmax,mcc} = \frac{N_{bat} I_{max} V_{nom}}{1000} \quad (8)$$

$$P_{bat,dmax,kbm} = \frac{kQ_i e^{-k\Delta t} + Qkc(1 - e^{-k\Delta t})}{1 - e^{-k\Delta t} + c(k\Delta t - 1 + e^{-k\Delta t})} \quad (9)$$

where $P_{bat,cmax}$ is the maximum charging power of the battery (kW), $P_{bat,cmax,kbm}$ is the maximum charging power of the battery within each time step (kW), $P_{bat,cmax,mcr}$ is the maximum charging power of the battery within the maximum charging rate limit (kW), $P_{bat,cmax,mcc}$ is the maximum charging power of the battery within the maximum charging current limit (kW), $P_{bat,dmax}$ is the maximum discharging power of the battery (kW), $P_{bat,dmax,kbm}$ is the maximum discharging power of the battery within each time step (kW), $\eta_{bat,c}$ is the battery charging efficiency, $\eta_{bat,d}$ is the battery discharging efficiency, Q_{max} is the maximum energy storage capacity of the battery (kJ), Q_i is the usable energy of the battery (kJ), Q is the usable energy of the battery (kJ), k is the rate constant of the battery, c is the capacity ratio of the battery, a_c is the maximum charging rate of the battery (Ah/h), N_{bat} is the total number of batteries in series and parallel, I_{max} is the maximum charging current of the battery (A), V_{nom} is the rated voltage of the battery (V).

2.5. Fuel Cell System Model

In this study, the fuel cell plays a critical role in the optimal configuration of the system. By properly designing the capacity of each component and simulating system performance under different operation strategies, an optimal balance between economic efficiency and reliability can be achieved.

The electrolyzer can electrolyze water into hydrogen and oxygen. Its output power can be expressed as follows:

$$P_{el\text{-}tank} = P_{el} \eta_{el} \quad (10)$$

where P_{el} is the input power of the electrolyzer, η_{el} is the efficiency of the electrolyzer, which is set to 60% in this paper.

The fuel cell is modeled as a proton exchange membrane fuel cell. The cell uses hydrogen as fuel and oxygen as the oxidant, converting chemical energy directly into electrical energy through electrochemical reactions. Its output power is expressed as follows:

$$P_{\mathrm{fc}} = P_{\text{tank-fc}}\eta_{\mathrm{fc}} \tag{11}$$

where $P_{\text{tank-fc}}$ is the power input from the hydrogen storage tank to the fuel cell, η_{fc} is the operating efficiency of the fuel cell.

3. Optimal Configuration Model of Off-Grid Microgrid-Based on HOMER

Based on the standard component models described above, this section further constructs a scenario-oriented optimization framework to compare the configuration results under different engineering objectives and operation strategies.

3.1. Optimization Objectives and Scenario Definition

3.1.1. Cleanliness Indicator

To reduce carbon emissions and improve renewable energy utilization, the cleanliness of the system is quantified by two indicators: renewable fraction (RF) and carbon dioxide emissions (E_{CO_2}). The calculation methods for the renewable fraction and non-renewable fraction of the off-grid microgrid system are as follows:

$$f_{RF} = 1 - f_{NRF} \tag{12}$$

$$f_{NRF} = \frac{E_{nonren}}{E_{served}} \times 100\% \tag{13}$$

where f_{RF} is the renewable fraction (RF), when f_{RF} is 0, it indicates that the electrical load in the microgrid is entirely supplied by fuel cells and diesel generators. Conversely, when f_{RF} is 1, it indicates that the electrical load in the microgrid is entirely supplied by distributed photovoltaics, f_{NRF} is the non-renewable fraction, E_{nonren} is the annual electricity generated by fuel cells and diesel generators in the microgrid system (kWh/a), E_{served} is the annual electrical load in the microgrid system (kWh/a).

As the system includes conventional distributed generation units, carbon dioxide emissions are inevitably generated during the operation of the microgrid. The calculation method is as follows:

$$E_{CO_2} = \eta P_{DG,t} \tag{14}$$

where E_{CO_2} is the CO_2 emissions generated by fuel cells and diesel generators in the off-grid photovoltaic–storage–fuel cell microgrid at time t (kg/kWh), $P_{DG,t}$ is the output power of fuel cells and diesel generators at time t (kW), and η is the carbon emission factor, taken as 0.86 kg/kWh.

3.1.2. Economic Indicator

To fully utilize photovoltaic power and reduce energy costs, the study adopts net present cost (NPC) and levelized cost of electricity (LCOE) as the basis for economic evaluation. LCOE is a comprehensive measure reflecting the unit cost of electricity generation over the entire life cycle of the system, and is calculated as follows:

$$f_{LCOE} = \frac{C_{ann,tot}}{E_{served}} \times 100\% \tag{15}$$

$$C_{ann,tot} = f_{NPC} \cdot C_{RN}(\rho, N) \tag{16}$$

$$C_{RN}(i, N) = \frac{\rho \cdot (1+\rho)^{\mathrm{N}}}{(1+\rho)^{\mathrm{N}} - 1} \tag{17}$$

where f_{LCOE} is the levelized cost of electricity of the system (CNY/kWh), $C_{ann,tot}$ is the annualized total cost of the system (CNY/a), f_{NPC} is the total net present cost of the system, including all costs and revenues incurred over the project lifetime, such as initial investment

costs, operation and maintenance costs, replacement costs, fuel costs, and salvage value (CNY), $C_{RN}(\rho, N)$ is the capital recovery factor, used to convert the present value into an equivalent annual cash flow. ρ is the discount rate, N is the lifetime of the project (a).

NPC refers to the difference between the present value of all costs and the present value of all revenues over the system's lifetime, and its calculation formula is as follows:

$$f_{NPC} = \frac{C_{ann,tot}}{C_{RN}(\rho, N)} \tag{18}$$

3.1.3. Optimization Objectives of Microgrid Under Multiple Scenarios

To optimize both the economic and environmental performance of the system, three scenarios are developed in this study. The specific objective functions for each scenario are as follows:

Scenario 1: Minimization of system net present cost. The objective function is as follows:

$$\min F_1 = f_{NPC} \tag{19}$$

Scenario 2: Maximization of the system's renewable fraction. The objective function is as follows:

$$\min F_2 = f_{NRF} \tag{20}$$

Scenario 3: Comprehensive optimization of system economic and environmental performance. The objective function is as follows:

$$\min F_3 = \omega_1 f_{LCOE} + \omega_2 f_{NPC} + \omega_3 f_{NRF} + \omega_4 E_{CO_2} \tag{21}$$

where $\omega_n (n = 1, 2, 3, 4)$ is the weight value corresponding to the n-th indicator.

In Scenario 3, the weights of the evaluation indicators in the comprehensive objective function are determined using the entropy weight method [8]. This method is an objective weighting approach that assigns weights according to the amount of information contained in each indicator. In general, an indicator with greater variation among different alternatives provides more discriminative information and therefore obtains a larger weight, whereas an indicator with smaller variation contributes less to the overall evaluation. The calculation procedure includes constructing the initial decision matrix, normalizing indicators with different dimensions and optimization directions, calculating the entropy and information utility of each indicator, and finally deriving the corresponding indicator weights [24]. The entropy weight method has been widely used in multi-criteria decision-making problems, and has also been applied to the multi-objective optimal design of stand-alone hybrid energy systems based on HOMER.

(1) Construction of the decision matrix. Based on the annual simulation results from HOMER Pro, each feasible capacity configuration is evaluated using indicators such as NPC, LCOE, non-renewable energy fraction, and CO_2 emissions. The calculated indicator values of all candidate configurations constitute the decision matrix. For m alternatives and n evaluation indicators, the matrix is defined as Equation (22).

$$A = (a_{ij})_{m*n} = \begin{pmatrix} a_{11} & \cdots & a_{1n} \\ \vdots & \ddots & \vdots \\ a_{m1} & \cdots & a_{mn} \end{pmatrix} \tag{22}$$

where a_{ij} is the index value of the j-th decision index of the i-th alternative solution.

(2) Normalization of the decision matrix. To eliminate the effects of different units and indicator directions, the original decision matrix is normalized before calculating

the indicator weights. Benefit-type and cost-type indicators are processed using Equations (23) and (24), respectively.

$$r_{\mathrm{ij}} = \frac{a_{\mathrm{ij}} - \min\limits_{j} a_{\mathrm{ij}}}{\max\limits_{j} a_{\mathrm{ij}} - \min\limits_{j} a_{\mathrm{ij}}} \tag{23}$$

$$r_{\mathrm{ij}} = \frac{\max\limits_{j} a_{\mathrm{ij}} - a_{\mathrm{ij}}}{\max\limits_{j} a_{\mathrm{ij}} - \min\limits_{j} a_{\mathrm{ij}}} \tag{24}$$

(3) Information entropy calculation. The information entropy of each indicator is calculated from the normalized decision matrix, as shown in Equation (25).

$$E_{\mathrm{j}} = -(\ln m)^{-1} \sum_{i=1}^{m} p_{ij} \ln p_{ij} \tag{25}$$

where E_{j} is the entropy value of indicator j, and p_{ij} is the normalized proportion of alternative i with respect to indicator j, as calculated by Equation (26).

$$p_{\mathrm{ij}} = \frac{r_{\mathrm{ij}}}{\sum\limits_{i=1}^{m} r_{\mathrm{ij}}} \tag{26}$$

(4) Determination of indicator weights. The weight ω_{j} of each evaluation indicator is calculated according to its information entropy, as expressed in Equation (27).

$$\omega_{\mathrm{j}} = \frac{1 - E_{\mathrm{j}}}{n - \sum\limits_{j=1}^{n} E_{\mathrm{j}}} \tag{27}$$

3.2. Operation Strategies and Control Logic Based on HOMER

3.2.1. LF Operation Strategy

In the photovoltaic–storage–fuel cell microgrid system constructed in this paper, the core logic of the Load Following operation strategy is as follows: photovoltaic power generation is prioritized to meet the load demand in real time, with any surplus electricity being used to charge the energy storage batteries. When the combined power supply from photovoltaics and storage is still insufficient, the fuel cell and diesel generator are activated according to the actual power deficit and operate in a load-following manner to avoid excess generation. This approach ensures power supply reliability while maximizing the renewable energy utilization rate and reducing fuel consumption and operating costs.

3.2.2. CC Operation Strategy

In the photovoltaic–storage–fuel cell microgrid system designed in this paper, the core logic of the cycle charging operation strategy is as follows: once the system determines that the fuel cell needs to be activated, it operates at its rated power once activated to improve generation efficiency. The generated power is allocated in the order of "critical loads—adjustable loads—lithium-battery charging", meaning that all electrical load demands are prioritized, and any surplus electricity is used to charge the energy storage batteries. When photovoltaic output is sufficient, the storage batteries can also be charged by photovoltaics. When the net load of the system is low (e.g., during nighttime or when photovoltaic output is high), the storage batteries can discharge to replace fuel cell operation, thereby reducing the number of start-stop cycles and inefficient operation time of the fuel cell, thus optimizing the system's economic performance. Through the peak-shaving and valley-

filling effect of the energy storage unit, this strategy enhances overall dispatch flexibility and reduces reliance on the real-time output of photovoltaics.

3.2.3. Comparative Analysis of Operation Strategies

This paper takes the microgrid system of a commercial and industrial park in Wuhan as the research object. Significant differences exist among different operation strategies in terms of applicable scenarios, operation mechanisms, cost control, and operating characteristics. The specific comparison is shown in Table 1.

Table 1. Comparison of operational strategy differences.

Comparison Dimension	LF Operation Strategy	CC Operation Strategy
Regions suitable for resource application	Regions with abundant renewable energy	Regions with scarce renewable energy
Core Operation Logic	Match load on demand, store surplus energy, controllable power sources serve as backup	Operate controllable power sources at rated output, allocate power in a prioritized manner, storage replaces generation when feasible
Function of Controllable Power Sources	Backup supplement, low start-up frequency	Primary power supply, long-term rated operation
Characteristics of Storage Operation	Dynamic charging and discharging, no fixed cycle	Cyclic charging and discharging, relies on surplus from controllable power sources
Key focus of cost control	Reduce start-up and operation costs of controllable sources	Improve operating efficiency of controllable sources, reduce unit energy cost

4. Case Study Analysis

4.1. Case Study Parameter Settings

4.1.1. Natural Resource and Load Parameter Settings

In this study, an off-grid photovoltaic–storage–fuel cell microgrid system located in a commercial park in Wuhan is selected as the case study object. The climatic conditions of the region significantly influence the configuration results: the annual sunshine duration ranges from 1800 to 2100 h, with annual total solar radiation between 104 and 113 kJ/cm^2. Solar irradiance exhibits a pattern of being higher in summer and lower in winter. The annual average temperature ranges from 15.8 to 17.5 °C, and low temperatures in winter may reduce battery efficiency. The annual solar irradiance and temperature distributions are shown in Figures 2 and 3. It should be noted that the natural resource data and load profile data shown in Figures 2–5 are adopted from a previously published Open Access study on a business park in Wuhan, China [25]. In this paper, these data are used as the basic case study inputs for further optimization analysis of the off-grid photovoltaic–storage–fuel cell microgrid under different operation strategies. Therefore, it is necessary to ensure a stable power supply to the park through reasonable scheduling of photovoltaics, fuel cells, and the energy storage system.

In this paper, the discount rate is set to 2%, and the diesel price is selected as 6.9 CNY/L. The initial investment and replacement cost of the selected photovoltaic modules are both 9599.2 CNY/kW, with a design life of 25 years. Their operating parameters are set as follows: derating factor of 80%, the photovoltaic system adopts a horizontal-axis continuous tracking mode, ground reflectance of 20%, temperature coefficient of −0.5, operating temperature of approximately 47 °C, and flat panel efficiency of 13%. In addition, the carbon emission intensity of the diesel generator in the microgrid is set to 1.98 g/L.

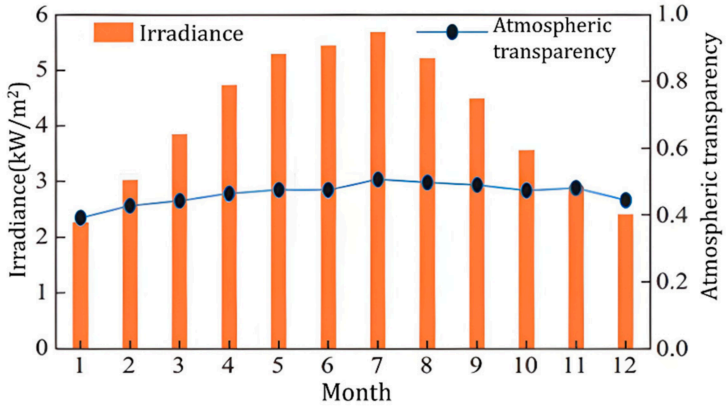


Figure 2. Annual solar irradiance distribution.

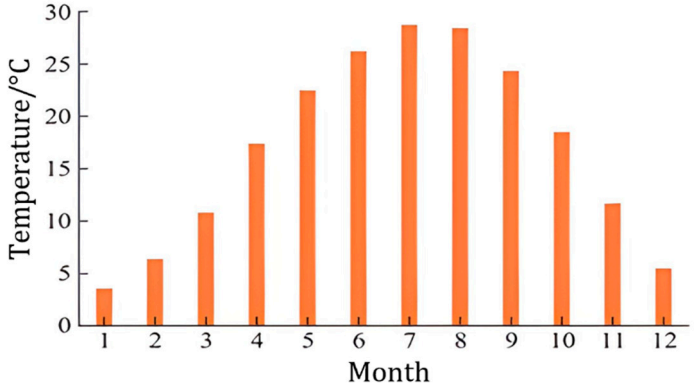


Figure 3. Annual temperature distribution.

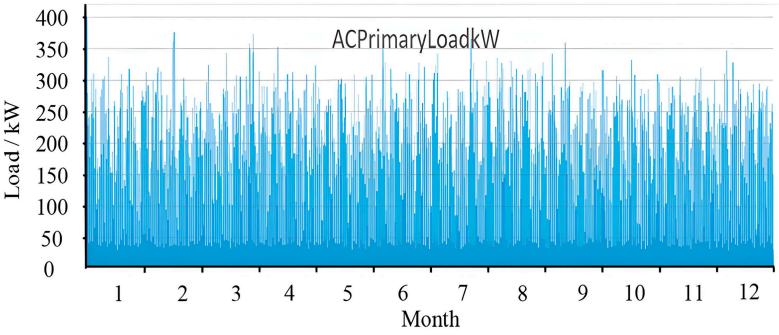


Figure 4. Annual load curve.

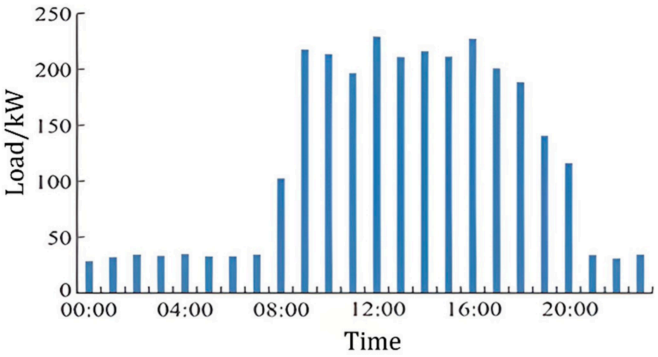


Figure 5. Typical daily load curve.

The load characteristics of the commercial park are as follows: the annual average daily electricity consumption is 2619.91 kWh, with a daily peak load of 376.19 kW. The

peak electricity usage period occurs from 09:00 to 20:00. The monthly average load ranges from 200 to 300 kW, with the peak electricity consumption occurring in August. The typical daily load curve and annual load curve are shown in Figures 4 and 5, respectively.

The above economic and technical assumptions were adopted based on the HOMER Pro component database, typical commercial device specifications, local market assumptions, and related HOMER-based microgrid studies. The discount rate of 2% is used for life-cycle economic assessment, while the diesel price of 6.9 CNY/L is set as the baseline fuel price for backup generation. Considering practical fuel price fluctuations, diesel prices of 7, 8, 9, and 10 CNY/L are further included in the sensitivity analysis. The photovoltaic cost, lifetime, and operating parameters are selected according to typical PV module specifications and previous microgrid planning studies.

4.1.2. Output Model Parameter Settings

The battery energy storage system is configured with a lithium-ion battery having a capacity of 100 kWh, and the rated voltage of the battery string is 600 V. The initial investment and replacement cost of the system are both 2000 CNY/kWh, and the annual operation and maintenance cost is 80 CNY/kWh.

The system design includes one 250 kW fuel cell system and one diesel generator with a fixed capacity of 100 kW. To improve the operating efficiency of the diesel generator and avoid excessively high operating costs under low-load conditions, its minimum operating load is restricted to 25%. The parameters of the generator and inverter are shown in Tables 2 and 3, respectively.

Table 2. Generator parameters.

Generator Type	Initial Investment and Replacement Cost (CNY/Unit)	Operation and Maintenance Cost (CNY/(h·Unit))
Fuel Cell Generator	250,000	80
Diesel Generator	40,000	9

Table 3. Inverter parameters.

Parameter Type	Parameter Value
Investment Cost (CNY/kW)	5393.54
Replacement Cost (CNY/kW)	4800
Annual Maintenance Cost (CNY/kW)	60
Operating Life (years)	15
Efficiency (%)	95

4.2. System Constraints

The operating constraints for each unit and the system are as follows:

(1) Photovoltaic output constraint.

$$0 \le P_{PV}(t) \le P_{PV,max} \tag{28}$$

where $P_{PV,max}$ is the maximum output power of the photovoltaic system, which is determined by the solar irradiance, temperature, and installed capacity (kW).

(2) Diesel generator output constraint.

$$P_{DG,min} \le P_{DG}(t) \le P_{DG,rated} \tag{29}$$

where $P_{DG,rated}$ is the rated power of the diesel generator (kW), $P_{DG,min}$ is the minimum output power of the diesel generator, which is set to 25% of its rated power in this paper.

(3) Fuel cell output constraint.

$$P_{fc,min} \leq P_{fc}(t) \leq P_{fc,rated} \quad (30)$$

where $P_{fc,rated}$ is the rated output power of the fuel cell (kW), $P_{fc,min}$ is the minimum output power of the fuel cell (kW).

(4) System power balance constraint

$$P_{PV}(t) + P_{fc}(t) + P_{DG}(t) + P_{dis}(t) - P_{ch}(t) = P_{load}(t) \quad (31)$$

where $P_{dis}(t)$ is the discharging power of the battery at time t (kW), $P_{ch}(t)$ is the charging power of the battery at time t (kW), $P_{load}(t)$ is the load demand of the system at time t (kW).

4.3. Optimal Configuration and Performance Comparison of Microgrid Under Different Operation Strategies

4.3.1. Impact of Different Operation Strategies on Optimal System Configuration

For Scenario 1 described in Section 3.1.3, the optimal configuration analysis under the LF and CC strategies was conducted, and the optimal configuration and power component parameter results under different strategies are presented in Table 4.

Table 4. Optimal configuration results of the microgrid system.

System Component	Performance Parameter	LF Strategy	CC Strategy
Photovoltaics	Installed Capacity (kW)	752	689
	Temperature Coefficient (°C)	−0.5	−0.5
	Derating Factor (%)	80	80
	Operating Temperature (°C)	47	47
	Lifetime (years)	25	25
	Efficiency (%)	13	13
Battery Bank	Nominal Capacity (kWh)	100	100
	Number of Battery Strings	15	16
	Battery Lifetime (years)	15	15
	Efficiency (%)	90	90
Inverter	Rated Power (kW)	308	310
	Lifetime (years)	15	15
	Efficiency (%)	95	95
Diesel Generator	Rated Output Power (kW)	100 × 1	0
	Minimum Load Ratio (%)	25	25
Fuel Cell Generator	Generation Capacity (kW)	250 × 1	250 × 1
	Minimum Load Ratio (%)	0	0
	Combined Heat and Power (CHP) Recovery Rate (%)	60	60
Boiler	Efficiency (%)	85	85

It can be observed that the photovoltaic installed capacity under the CC strategy is lower than that under the LF strategy. This is because the CC strategy prioritizes the use of the energy storage system for cyclic charging and discharging to smooth power fluctuations. With a larger capacity of 16 battery strings, it reduces the reliance on real-time photovoltaic power supply. Meanwhile, the generator operation mode under the CC strategy is more flexible and does not require continuous operation at rated power to compensate for photovoltaic output deficits, thereby reducing the demand for photovoltaic installed capacity.

Table 5 presents the comparison results of system economic and cleanliness indicators under the two strategies. In terms of economic performance, both the NPC and LCOE

under the CC strategy are lower than those under the LF strategy, indicating superior economic performance. Regarding cleanliness, the RF value under the CC strategy is 8.1% lower than that under the LF strategy, and the E_{CO_2} value is also reduced by 0.35%. Overall, the LF strategy not only exhibits inferior economic performance but also has a loss of power supply probability (LPSP) of 0.033%, failing to fully guarantee power supply reliability. Therefore, for the off-grid photovoltaic–storage–fuel cell microgrid constructed in this paper, the CC strategy is the preferable choice.

Table 5. Comprehensive assessment of economic and cleanliness indicators for the two operational strategies.

Strategy	NPC (10,000 CNY)	LCOE (CNY/kWh)	RF (%)	E_{CO_2} (kg/a)
LF	16,558.84	1.31	84.2	2,882,731
CC	16,541.20	1.30	77.4	2,872,507

Technically, the main difference between the LF and CC strategies lies in the coordination among photovoltaic generation, controllable generators, and battery storage. Under the LF strategy, the fuel cell and diesel generator mainly compensate for the instantaneous net load deficit, so the system depends more on photovoltaic capacity to reduce backup generation. In contrast, under the CC strategy, the controllable generator can operate at a relatively high output once started, and surplus power is stored in the battery. This improves battery utilization and reduces the need for excessive photovoltaic capacity, explaining why the CC strategy achieves a lower PV capacity with better economic performance in this case.

Tables 6 and 7 list the initial investment, replacement, operation and maintenance, fuel, and salvage costs of each system component under the two strategies, respectively. In terms of overall cost, the total cost of the optimal configuration under the CC strategy is lower than that under the LF strategy. Specifically, the LF strategy incurs higher initial investment and fuel costs, whereas the CC strategy, due to the increased number of battery strings and the continuous operation of the generator at rated power, results in more frequent fuel cell output and battery charging, leading to correspondingly higher battery operation, maintenance, and replacement costs.

To further clarify the output characteristics of the system under different operation strategies, this paper analyzes the annual operation curves of each unit. Figure 6 shows the diesel consumption characteristics under different operation strategies. Specifically, Figure 6a and 6b present the annual diesel consumption and monthly diesel consumption under the LF strategy, respectively, while Figure 6c and 6d present the annual diesel consumption and monthly diesel consumption under the CC strategy, respectively. During days 120 to 240 of the year, the fuel expenditure of the system exhibits a significant decline. This phenomenon is mainly attributed to the peak solar irradiance in summer, which substantially increases photovoltaic power generation. With relatively stable load demand, the system's reliance on diesel generators for supplementary power supply decreases, thereby reducing fuel consumption. Photovoltaic output can preferentially meet the electricity demand of the park, and any surplus electricity can be stored in the energy storage batteries, thus reducing the electricity cost of the park. To minimize the system net present cost (NPC), the LF strategy prioritizes the activation of the 250 kW fuel cell system to operate at rated power when photovoltaic output falls below the load demand. This activation strategy is designed to precisely meet the load while avoiding excess electricity generation, resulting in a higher proportion of electricity generated by the fuel cell compared to the CC strategy. The comparison shows that the annual diesel consumption under the LF and CC

strategies is 1,090,827 L and 1,086,936 L, respectively. Although an additional 100 kW diesel generator is deployed in the LF strategy, it only serves to follow the net load for regulation purposes, resulting in diesel consumption that is only about 0.35% higher than that under the CC strategy.

Table 6. Costs of each component in the microgrid system under the LF strategy.

System Component	Initial Investment (10,000 CNY)	Replacement Cost (10,000 CNY)	O&M Cost (10,000 CNY)	Fuel Cost (10,000 CNY)	Salvage Cost (10,000 CNY)	Total Cost (10,000 CNY)
100 kWh Lithium-ion Battery Bank	300.00	222.90	23.43	0	60.95	485.38
250 kW Fuel Cell	250.00	0	139.94	369.33	84.11	675.16
100 kW Diesel Generator	4.00	9.38	41.54	337.80	0.15	392.58
Photovoltaics	721.52	0	14.67	0	0	736.19
Inverter	166.07	109.81	36.06	0	30.03	281.91
Boiler	0	0	0	13,987.60	0	13,987.60
System	1441.59	342.09	255.65	14,694.74	175.24	16,558.84

Table 7. Costs of each component in the microgrid system under the CC strategy.

System Component	Initial Investment (10,000 CNY)	Replacement Cost (10,000 CNY)	O&M Cost (10,000 CNY)	Fuel Cost (10,000 CNY)	Salvage Cost (10,000 CNY)	Total Cost (10,000 CNY)
100 kWh Lithium-ion Battery Bank	320.00	238.25	24.99	0	62.75	520.49
250 kW Fuel Cell	250.00	0	216.47	818.26	46.78	1237.95
Photovoltaics	661.12	0	13.45	0	0	674.56
Inverter	167.37	110.66	36.35	0	30.26	284.12
Boiler	0	0	0	13,824.06	0	13,824.06
System	1398.49	348.92	291.26	14,642.32	139.79	16,541.20

The key photovoltaic output indicators under the two strategies are shown in Table 8. Under the LF strategy, the renewable energy capacity ratio is 68.2%, and the monthly power generation distribution from each source is shown in Figure 7a. The data show that the ratio of annual photovoltaic power generation to total annual system load demand reaches 113%, and the photovoltaic penetration rate also reaches 84.2%, fully indicating that photovoltaic energy is the core power source of the microgrid. As supplementary power supply units, the fuel cell generator and diesel generator are primarily activated during peak electricity demand periods to ensure a stable power supply. Under the LF strategy, the annual curtailed photovoltaic power reaches 260,047 kWh (accounting for 20.2% of the total power generation), with an annual load power deficit of approximately 587 kWh. Under the CC strategy, the renewable energy capacity accounts for 73.4% of the total capacity, and the monthly power generation from different sources is shown in Figure 7b. Under the CC strategy, photovoltaic power generation can meet 104% of the annual system load demand, with a photovoltaic penetration rate of 77.4%. However, this strategy still incurs certain energy losses and power supply gaps, with annual curtailed

photovoltaic power of 248,275 kWh (19.4% of the total power generation) and an annual unmet load of approximately 96.3 kWh.

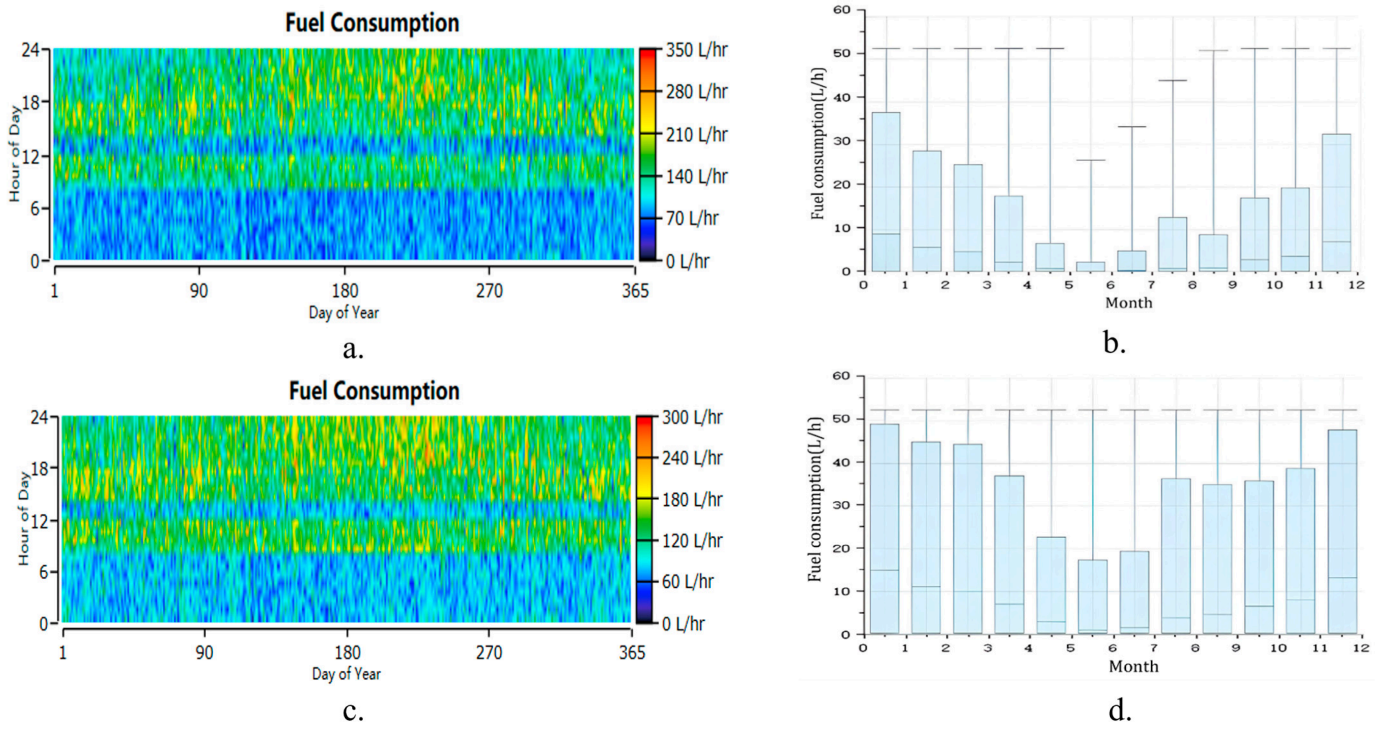


Figure 6. Diesel consumption comparison under different operation strategies: (**a**) annual diesel consumption under the LF strategy; (**b**) monthly diesel consumption under the LF strategy; (**c**) annual diesel consumption under the CC strategy; (**d**) monthly diesel consumption under the CC strategy.

Table 8. PV output parameters.

Photovoltaic Output Parameter	LF Strategy	CC Strategy
Maximum Output Power (kW)	578	530
Photovoltaic Penetration Rate (%)	84.2	77.4
Operating Hours (h/a)	4380	4380
Levelized Cost of Photovoltaic Electricity (CNY/kWh)	0.35	0.335

Figures 8 and 9 show the annual state of charge (SOC) distribution curves of the battery under the two strategies, respectively. Under the LF strategy, the lithium-ion battery energy storage system exhibits high-frequency charging and discharging characteristics. Analysis indicates that from day 90 to day 270 of the year, the duration during which the battery remains at full state of charge increases significantly, likely due to photovoltaic power generation far exceeding the actual electricity load. During the midday period, the battery SOC generally remains above 90%. Constrained by the energy storage capacity, surplus photovoltaic power cannot be stored, thereby exacerbating the curtailment issue. Under the CC strategy, during days 90 to 270, the lithium-ion battery bank remains at a relatively high state of charge, and the utilization rate of the energy storage system is significantly improved. This occurs because when the photovoltaic power supply is insufficient, the fuel cell system operates at rated power. In addition to meeting system load demand, the surplus electricity is promptly stored in the battery, resulting in high SOC levels during the early morning and evening periods. In contrast, under the LF strategy, the battery SOC remains at a consistently low level during the same period. Since the fuel cell system and

diesel generator under this strategy only supply power to cover the net load deficit, they generate almost no excess electricity, which helps extend the battery service life.

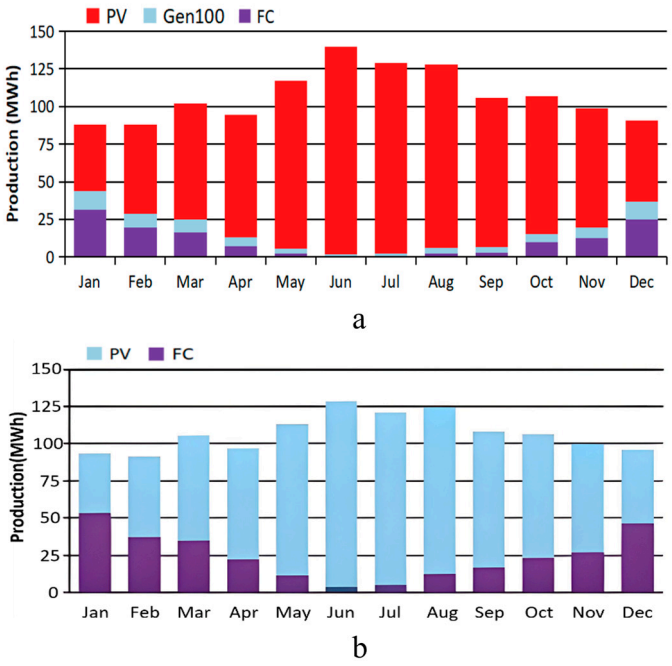


Figure 7. Monthly power generation from each power source under different operation strategies: (**a**) LF strategy; (**b**) CC strategy.

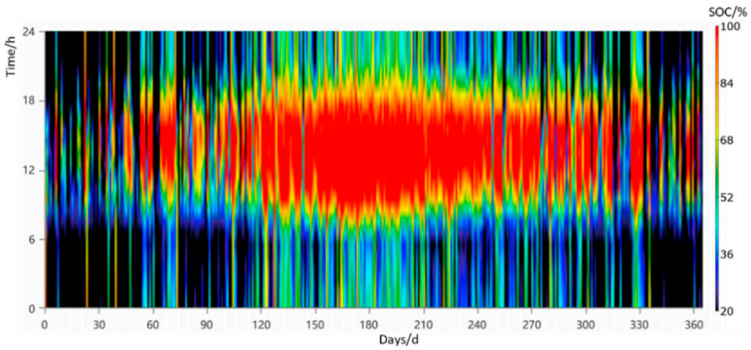


Figure 8. SOC of the battery under the LF strategy.

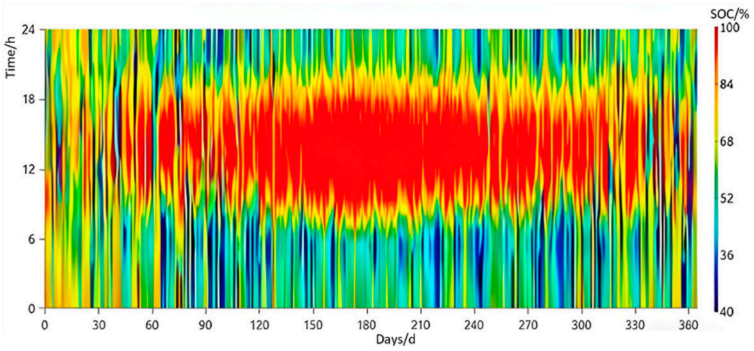


Figure 9. SOC of the battery under the CC strategy.

4.3.2. Multi-Scenario Optimal Configuration Results

To determine the weights of each indicator in Scenario 3, this paper adopts a data-driven objective weighting method—the entropy weight method. Its core principle is to quantify indicator uncertainty through information entropy, which is negatively correlated

with data dispersion. The lower the information entropy of an indicator, the higher the dispersion, the greater the effective information content, and thus the higher the weight. If the indicator values are completely identical, the indicator is excluded. The implementation process of this method involves: constructing a decision matrix, normalizing the data (to eliminate dimensional effects), calculating the information entropy of each indicator, and determining the weights based on information entropy and dispersion characteristics, thereby providing weight support for the multi-objective function.

Based on the scenarios defined in Section 3.1.3, this study constructs multi-scenario models and conducts optimal configuration analysis for the off-grid photovoltaic–storage–fuel cell microgrid system. Table 9 presents the weight results of each indicator calculated using the entropy weight method in Scenario 3.

Table 9. Indicator weights in the microgrid system.

Indicator	Information Entropy Value	Information Utility Value	Weight (%)
NPC (10,000 CNY)	0.994	0.006	13.281
LCOE (CNY/kWh)	0.994	0.006	13.278
RF (%)	0.985	0.015	36.187
E_{CO_2}/(kg/a)	0.984	0.016	37.254

The optimal system configuration results under each scenario are shown in Table 10. Scenario 1 achieves the best economic performance (lowest NPC and LCOE) but exhibits poor cleanliness. Scenario 2 takes RF maximization as the primary objective, achieving a renewable fraction (RF) of 99.8%, which is 22.4% higher than that of Scenario 1, but at the cost of poorer economic performance. To achieve this goal, the installed capacities of photovoltaics and lithium-ion batteries are 2.8 times and 1.06 times those of Scenario 1, respectively, resulting in NPC and LCOE that are 11.44% and 77.69% higher, respectively. Scenario 3 comprehensively considers both economic performance and cleanliness. Although its NPC and LCOE are slightly higher than those of Scenario 1, the renewable fraction is significantly improved. Compared with Scenario 2, its NPC and LCOE are substantially reduced, and the lithium-ion battery capacity is decreased by 65%, reducing the reliance on energy storage batteries. Thus, Scenario 3 achieves the best trade-off between cost and environmental benefits.

Table 10. The optimal configuration results for the three scenarios of the microgrid system.

Configuration Parameter	Scenario 1	Scenario 2	Scenario 3
Photovoltaic Rated Power (kW)	689	2620	1238
Lithium Battery Capacity (kWh)	1600	3300	2000
NPC (10,000 CNY)	16,541.20	18,433.20	16,907.22
LCOE (CNY/kWh)	1.30	2.31	1.50
RF (%)	77.4	99.8	95.8
E_{CO_2}/(kg/a)	2,872,507	2,773,247	2,797,909

The configuration differences among the three scenarios reflect the trade-off between renewable energy utilization and investment cost. Scenario 1 limits PV and battery capacities to minimize NPC, while Scenario 2 requires much larger PV and battery capacities to maximize RF, leading to higher investment and LCOE. Scenario 3 balances economic and environmental indicators, allowing the fuel cell and battery to jointly provide flexibility support and maintain a high RF without excessive battery oversizing.

The optimal configuration obtained in Scenario 3 was compared with a conventional PV-storage scheme under the same load demand, meteorological resource conditions,

project lifetime, and power supply reliability requirement. The conventional PV-storage scheme refers to a system consisting only of photovoltaic generation and lithium-ion battery storage, without the fuel cell unit. Based on the HOMER optimization results, the NPC reduction rate and battery capacity reduction rate were calculated as follows:

$$\text{NPC reduction rate} = (\text{NPC of conventional PV-storage scheme} - \text{NPC of proposed PV-storage-fuel cell scheme})/\text{NPC of conventional PV-storage scheme} \times 100\%$$

$$\text{Battery capacity reduction rate} = (\text{Battery capacity of conventional PV-storage scheme} - \text{Battery capacity of proposed PV-storage-fuel cell scheme})/\text{Battery capacity of conventional PV-storage scheme} \times 100\%$$

As shown in Table 10, the proposed PV-storage-fuel cell scheme under Scenario 3 has an NPC of 169.0722 million CNY, an RF of 95.8%, and a lithium-ion battery capacity of 2000 kWh. Compared with the conventional PV-storage scheme, the NPC is reduced by approximately 14.4%, and the lithium-ion battery capacity is reduced by approximately 24.3%. These results indicate that the introduction of the fuel cell unit can reduce the dependence on lithium-ion battery capacity while maintaining a high renewable fraction and improving the comprehensive economic performance of the system.

4.4. Sensitivity Analysis Results

Factors such as diesel fuel price, initial investment costs of photovoltaic modules and batteries, and load demand significantly affect the optimal configuration results of the off-grid photovoltaic–storage–fuel cell microgrid. Therefore, this section conducts a sensitivity analysis of the aforementioned factors, with the specific parameter settings shown in Table 11.

Table 11. Parameter settings for sensitivity analysis of the microgrid system.

Sensitivity Analysis Parameter	Value
Diesel Price (CNY/L)	7, 8, 9, 10
Initial Cost Multiplier of Photovoltaic Modules	0.6, 1.0
Initial Cost Multiplier of Batteries	0.6, 1.0
Load (kWh/d)	2619.19, 3000, 3500, 4000

When the initial cost multipliers of photovoltaic modules and lithium batteries are both fixed at 1.0, Figure 10 illustrates the impact of different diesel prices and load demands on the microgrid system configuration.

As shown in Figure 10, when the diesel price ranges from 7.3 to 8.0 CNY/L with a load demand of 2680–3050 kWh/d, and when the diesel price ranges from 8.5 to 8.9 CNY/L with a load demand of 3100–3250 kWh/d, the optimal configuration includes one additional 100 kW diesel generator with a fixed capacity compared with other cases. When the initial cost multipliers of photovoltaic modules and lithium batteries are both fixed at 0.6, the optimal system configuration remains unchanged within the considered ranges of diesel price and load demand. This result indicates that lower photovoltaic and battery costs improve the stability of the optimal configuration and reduce the sensitivity of capacity configuration to diesel price and load demand variations. However, regardless of the initial cost multiplier settings, the system NPC still shows an increasing trend with the increase in diesel price and load demand.

This result indicates that the optimal configuration is mainly determined by the cost competitiveness among photovoltaic generation, battery storage, and diesel backup generation. When PV and battery costs are high, the system becomes more sensitive to diesel price and load growth. As PV and battery costs decrease, renewable generation and

storage become more economically attractive, making the configuration more stable under fuel price fluctuations.

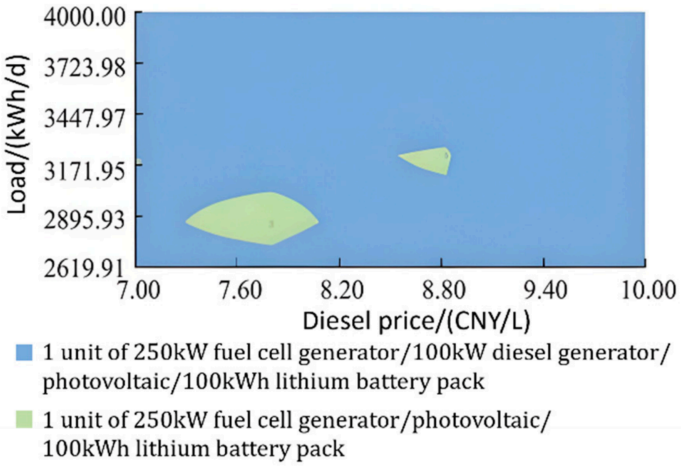


Figure 10. The cost multiplier is 1.0.

5. Conclusions

In this paper, an optimal design study of an off-grid photovoltaic–storage–fuel cell system is conducted based on HOMER Pro. First, the optimal system configurations under the LF and CC operation strategies are analyzed, and the adaptability of the operation strategies under this scenario is clarified. Based on the analysis of system configuration, photovoltaic penetration rate, and energy storage operation characteristics under specific operation strategies, as well as a comprehensive comparison of economic and cleanliness indicators and the sensitivity of key factors, this study draws the following main conclusions:

(1) Based on the selected research scenario and taking the minimization of system net present cost (NPC) as the objective, a comparison of the system configuration schemes under the two operation strategies reveals that the CC strategy is more suitable for the current scenario. The optimal system composition under the CC strategy consists of a 689 kW photovoltaic array, one 250 kW fuel cell generator, a 310 kW inverter, and 16 battery strings, each with a capacity of 100 kWh. Under the off-grid operation mode, a relatively high photovoltaic capacity is configured to mitigate the fluctuation of photovoltaic output, which, to some extent, also leads to the occurrence of photovoltaic curtailment.

(2) Using economic performance and cleanliness as evaluation indicators, this paper analyzes the optimal system configurations under different optimization objective scenarios. Scenario 1, which solely aims at minimizing the NPC, results in a relatively low renewable fraction and poor system cleanliness. Scenario 2 focuses on improving the renewable fraction, which leads to inferior economic performance, with a levelized cost of electricity (LCOE) as high as 2.31 CNY/kWh. Based on a comprehensive trade-off between system economic cost and environmental benefits, the optimal configuration scheme finally determined for Scenario 3 is as follows: a photovoltaic installed capacity of 1238 kW and a lithium battery energy storage capacity of 2000 kWh. Under this scenario, the renewable fraction is significantly improved, while the NPC and LCOE are only 2.2% higher than those of Scenario 1.

(3) The photovoltaic–storage–fuel cell microgrid system demonstrates superiority in cleanliness indicators, achieving a maximum renewable fraction (RF) of 99.8%, stronger renewable energy accommodation capability, and significantly reduced carbon emissions. In terms of long-term economic performance, Scenario 3 has an NPC of 169.0722 million CNY and an LCOE of 1.5 CNY/kWh. Although these values are

slightly higher than those of other scenarios, under conditions of rising diesel prices, Scenario 3 not only ensures high cleanliness but also reduces dependence on fossil fuels and energy storage degradation, mitigates the risk of long-term operating cost fluctuations, and achieves a better trade-off between the dual objectives of "cleanliness and economy".

Nevertheless, this study still has some limitations. First, the case study is based on the resource conditions and load characteristics of a commercial park in Wuhan, so the applicability of the conclusions to other regions or different load types requires further verification. Second, the optimization is conducted at the planning level using HOMER Pro, while real-time operational data and dynamic dispatch control are not further considered. Future work will extend the analysis to more application scenarios and incorporate actual operation data to improve the engineering applicability of the proposed configuration scheme.

Author Contributions: Conceptualization, H.M. and K.Z.; methodology, H.M., K.Z. and J.Y. (Jie Yang); software, H.M., K.Z. and J.Y. (Jie Yang); validation, H.M., K.Z. and J.Y. (Jie Yang); formal analysis, H.M. and J.Y. (Jie Yang); investigation, J.Y. (Jie Yang) and W.Y.; resources, W.Y., L.L. and Y.W.; data curation, W.Y. and L.L.; writing—original draft, H.M.; writing—review and editing, J.Y. (Jilei Ye); visualization, L.L. and Y.W.; supervision, L.L., Y.W. and J.Y. (Jilei Ye); project administration, W.Y., L.L., Y.W. and J.Y. (Jilei Ye); funding acquisition, W.Y. and J.Y. (Jilei Ye). All authors have read and agreed to the published version of the manuscript.

Funding: This research was funded by the Basic Research Program of Jiangsu (BK20250608).

Data Availability Statement: The data presented in this study are available on request from the corresponding author. The data are not publicly available due to their use in projects belonging to state-owned enterprises.

Conflicts of Interest: The authors declare no conflicts of interest.

References

1. Qi, W.; Geng, S.B.; Gao, H.S. Design of solar hybrid power generation system based on HOMER simulation. *Electrotech. Electr.* **2011**, *8*, 27–32. Available online: https://kns.cnki.net/kcms2/article/abstract?v=gW15YWgIns2seVoprKUSGLmh7anIxKRBKPE5zYqOuax9IuMJrNwfKVaH7X8WdbZqSti1S57dWVRzRuqSiJlSMyp_J6UH-bCZWUy3YC817vZ8-yHzEUeVHHhrgTcCvFwR3uTkv22Q0G1bRWxEt5lJnyqGfDMS_M07&uniplatform=NZKPT (accessed on 5 March 2026).
2. Yang, T.; Cui, G.L. Research on optimal capacity configuration of off-grid wind-solar-diesel-storage microgrid. *Green Pet. Petrochem.* **2025**, *10*, 44–51. Available online: https://kns.cnki.net/kcms2/article/abstract?v=gW15YWgIns2eEDTMTX44AO-fKY1ccaXPieDRAt7BZ1VguVZUeuLyavHLaL-BlT3LG3Myas-rmaGy_MS-Kscc_H3GRIBA40dI86Kq136Z7H8yRKZQa4g0p0oNlQFyPtqgjGtHyWKgeIxhFLu0qqxJ_7HmMXBLR789lSOj0rtglYc=&uniplatform=NZKPT (accessed on 7 March 2026).
3. Khodayar, M.E. Rural electrification and expansion planning of off-grid microgrids. *Electr. J.* **2017**, *30*, 68–74. [CrossRef]
4. Zhang, Z.H. Cost Analysis and Countermeasure Research of Microgrid Projects. Master's Thesis, Tianjin University, Tianjin, China, 2017. Available online: https://kns.cnki.net/kcms2/article/abstract?v=gW15YWgIns30aRzIFh4H4ec6_obWcyNVLzBgi2RSkpt0h6bxcxYKdChJW553e6O6w_1WURG8dcZ6w_7Lsw3ZpscxKhO5NXmqoYH5482Esb-6p3t9v6_95VfLdc21fkbywI6yeuhabqXGixWnGBEPr5IjavfZXvyF6KF-pYSZYVk=&uniplatform=NZKPT (accessed on 6 March 2026).
5. Li, C.P.; Zhang, T.Y.; Zhou, F. A review of solar photovoltaic power generation. *Electr. Eng. Mater.* **2006**, *3*, 45–48. Available online: https://jghj.cbpt.cnki.net/portal/journal/portal/client/paper/19afbd6df200635c5ca2e716e345e22e (accessed on 9 March 2026).
6. Luo, Y. Research on Multi-Indicator Evaluation of Integrated Energy Systems Based on AHP-Entropy Weight Method. Master's Thesis, North China Electric Power University, Beijing, China, 2021. Available online: https://kns.cnki.net/kcms2/article/abstract?v=gW15YWgIns1usf-k0JiT6jAv9EDoiuKuUQ0MZ2GEqKEvWeGgrSwYQRTjfrpZsR50E_ISoU7o7LmYVEldwiW4urWg4-p7cVRKL32KEatsBtyOWJqSd5exC5Quo6eN5HlJ5kpaEa9N0fG7-W8Epv_cieTQaoVUp2ycpVwDi58gOoY=&uniplatform=NZKPT (accessed on 8 March 2026).
7. Liu, M.L. Research on Environmental-Economic Dispatch Model and Optimization Algorithm for Microgrid Systems. Master's Thesis, North China Electric Power University, Beijing, China, 2014. Available online: https://kns.cnki.net/kcms2/article/abstract?v=gW15YWgIns0-UMQx-sM4f2xGqV-mDfAj8HpmRO7DeuTLpETtSzZbj97fSE0LyeDCMCJ8XkZ0WYv_UdVadmzOUSJd5qR1bXcsos_XMdJeYviB_6K1QYNdATn74y5HBNqS1whoY-7vVKoW0mbyPHS35EIJwj0TqSolYDIXXdvCWe4=&uniplatform=NZKPT (accessed on 10 March 2026).

8. Lu, J.X.; Wang, W.J.; Zhang, Y.C. Multi-objective optimal design of stand-alone hybrid energy system using entropy weight method based on HOMER. *Energies* **2017**, *10*, 1664. [CrossRef]
9. Zhang, Y.Z. Evaluation of Adjustable Value and Aggregation Analysis of Distribution Network Loads. Master's Thesis, Nanjing University of Posts and Telecommunications, Nanjing, China, 2022. Available online: https://vpnlib.njtech.edu.cn/https/webvpnbf86c07c4d77b5ce3ef42b2a43d33a266570bf5dc99793155c3ffe8ee1ff9d4f/thesis/Ch1UaGVzaXNOZXdTb2xyOVMyMDI2MDUxMjA3Mjk0NxIJRDAyODUwMDY3GghnNW5zNnM5dQ%3D%3D (accessed on 11 March 2026).
10. Dong, Q.; Xu, J.; Fang, D.P. Optimal scheduling strategy of distributed PV-storage systems based on PV output characteristics. *Integr. Intell. Energy* **2024**, *46*, 17–23. Available online: https://kns.cnki.net/kcms2/article/abstract?v=gW15YWgIns0QQxdlf7ZB-eGyldtYUHrVX5aw6HOs3BObYU1gVK3vaLPi9Wv7ccc0DWYqExDNMxsy4V7fyWjNKi4aotSLiDw7e-dKAjFIEV7hnTkXkpD8aFtkjEWRCPggWQShJNZAMHL0wP5-yUmFRRtuPRfbWvTUXvw-uUkXpH4=&uniplatform=NZKPT (accessed on 14 March 2026).
11. Yu, G.X.; Li, Z.W.; Jin, S.J. Research on optimal energy scheduling strategy for smart communities based on photovoltaics and batteries. *Process Autom. Instrum.* **2022**, *43*, 21–27. Available online: https://kns.cnki.net/kcms2/article/abstract?v=gW15YWgIns2zEdZPkWorEnxMVVY9rivDgLNPua7YuLU5wQoVKX6smru9VzfnI4BZXYSiXFT9H3BT1BShtPV8Id4rh9um6tK6_micNiWSnSElywuGFiZX_DO6XuqFveb54oPxD8L1cMmFAOGDjuBPgCY2C6fw3jxIDmoh1IKOVVQ=&uniplatform=NZKPT (accessed on 12 March 2026).
12. Zhang, Y.F.; Yan, S.Y.; Li, B. Optimal design of off-grid microgrids under multiple scenarios based on HOMER. *Acta Energiae Solaris Sin.* **2024**, *45*, 123–134.
13. Laetitia, U.; Hyun-Goo, K.; Chang, K.K. Feasibility study of integrating the renewable energy system in Popova Island using the Monte Carlo model and HOMER. *Energy Strategy Rev.* **2021**, *33*, 100607. [CrossRef]
14. Bahramara, S.; Moghaddam, M.P.; Haghifam, M.R. Optimal planning of hybrid renewable energy systems using HOMER: A review. *Renew. Sustain. Energy Rev.* **2016**, *62*, 609–620. [CrossRef]
15. Halabi, L.M.; Mekhilef, S.; Olatomiwa, L. Performance analysis of hybrid PV/diesel/battery system using HOMER: A case study Sabah, Malaysia. *Energy Convers. Manag.* **2017**, *144*, 322–339. [CrossRef]
16. Karakoulidis, K.; Mavridis, K.; Bandekas, D.V. Techno-economic analysis of a stand-alone hybrid photovoltaic-diesel-battery-fuel cell power system. *Renew. Energy* **2011**, *36*, 2238–2244. [CrossRef]
17. Shaahid, S.M.; El-amin, I. Techno-economic evaluation of off-grid hybrid photovoltaic-diesel-battery power systems for rural electrification in Saudi Arabia-a way forward for sustainable development. *Renew. Sustain. Energy Rev.* **2009**, *13*, 625–633. [CrossRef]
18. Hafez, O.; Bhattacharya, K. Optimal planning and design of a renewable energy based supply system for microgrids. *Renew. Energy* **2012**, *45*, 7–15. [CrossRef]
19. Chauhan, A.; Saini, R.P. A review on Integrated Renewable Energy System based power generation for stand-alone applications: Configurations, storage options, sizing methodologies and control. *Renew. Sustain. Energy Rev.* **2014**, *38*, 99–120. [CrossRef]
20. Jung, J.; Villaran, M. Optimal planning and design of hybrid renewable energy systems for microgrids. *Renew. Sustain. Energy Rev.* **2017**, *75*, 180–191. [CrossRef]
21. Ishraque, M.F.; Shezan, S.A.; Ali, M.M.; Rashid, M.M. Optimization of load dispatch strategies for an islanded microgrid connected with renewable energy sources. *Appl. Energy* **2021**, *292*, 116879. [CrossRef]
22. Zhao, C.L. Research on the Economic Operation of Microgrids and the Application of HOMER Software. Master's Thesis, Southwest Jiaotong University, Chengdu, China, 2015. Available online: https://kns.cnki.net/kcms2/article/abstract?v=gW15YWgIns2eKy1sKpMlVsQ_5mfKIq7qh0-Br4nUx09o5uzVTL_5XoUHpT9zsejjxysrZSfk7tGqKiVg9E78Tgh2dKi15NfpLed251fhdhv0T_o-nwOwUOCDkdvkwoaqGMLr6bP3FM34V28VLjuG09Po0p6mavCv_Bq61OXbRHk=&uniplatform=NZKPT (accessed on 17 March 2026).
23. Jiang, C.C. Research on Optimal Design and Economic Dispatch of Stand-Alone Microgrid Systems. Master's Thesis, Wuhan University of Technology, Wuhan, China, 2019. Available online: https://kns.cnki.net/kcms2/article/abstract?v=gW15YWgIns1M-G6BwhyOJ65WlNa71b-Nz0a0Pwl7t0_Oc3htQhDA7o76Mc6u0NwFwbRiPitU9ilAWLGdwUfF26rhO02EtbATB1raW8jAi0qoHbvY3hyez3Zuqgf3WiVEdGp0XQFnhxqTCHIUnZ636Qj-aijttEqbhKQ3NeAEKt8=&uniplatform=NZKPT (accessed on 20 March 2026).
24. Zhu, Y.; Tian, D.; Yan, F. Effectiveness of Entropy Weight Method in Decision-Making. *Math. Probl. Eng.* **2020**, *2020*, 3564835. [CrossRef]
25. Zhang, Y.F.; Yan, S.Y.; Yin, W.Q.; Wu, C.; Ye, J.L.; Wu, Y.P.; Liu, L.L. HOMER-Based Multi-Scenario Collaborative Planning for Grid-Connected PV-Storage Microgrids with Electric Vehicles. *Processes* **2023**, *11*, 2408. [CrossRef]

Disclaimer/Publisher's Note: The statements, opinions and data contained in all publications are solely those of the individual author(s) and contributor(s) and not of MDPI and/or the editor(s). MDPI and/or the editor(s) disclaim responsibility for any injury to people or property resulting from any ideas, methods, instructions or products referred to in the content.